ORIGINAL ARTICLE

JBMR®

Bone Microarchitecture Assessed by HR-pQCT as Predictor of Fracture Risk in Postmenopausal Women: The OFELY Study

Elisabeth Sornay-Rendu,* Stephanie Boutroy,* François Duboeuf, and Roland D Chapurlat

INSERM UMR 1033 and Université de Lyon, Lyon, France

ABSTRACT

Several cross-sectional studies have shown that impairment of bone microarchitecture contributes to skeletal fragility. The aim of this study was to prospectively investigate the prediction of fracture (Fx) by bone microarchitecture assessed by high-resolution peripheral computed tomography (HR- pQCT) in postmenopausal women. We measured microarchitecture at the distal radius and tibia with HR-pQCT in the OFELY study, in addition to areal BMD with dual-energy X-ray absorptiometry (DXA) in 589 women, mean ± SD age 68 ± 9 years. During a median [IQ] 9.4 [1.0] years of follow-up, 135 women sustained an incident fragility Fx, including 81 women with a major osteoporotic Fx (MOP Fx). After adjustment for age, women who sustained Fx had significantly lower total and trabecular volumetric densities (vBMD) at both sites, cortical parameters (area and thickness at the radius, vBMD at the tibia), trabecular number (Tb.N), connectivity density (Conn.D), stiffness, and estimated failure load at both sites, compared with control women. After adjustment for age, current smoking, falls, prior Fx, use of osteoporosis-related drugs, and total hip BMD, each quartile decrease of several baseline values of bone microarchitecture at the radius was associated with significant change of the risk of Fx (HR of 1.39 for Tb.BMD [$p = 0.001$], 1.32 for Tb.N [$p = 0.01$], 0.76 for Tb.Sp.SD [$p = 0.01$], 1.49 [$p = 0.01$] for Conn.D, and 1.27 for stiffness [$p = 0.02$]). At the tibia, the association remained significant for stiffness and failure load in the multivariate model for all fragility Fx and for Tt.BMD, stiffness, and failure load for MOP Fx. We conclude that impairment of bone microarchitecture—essentially in the trabecular compartment of the radius—predict the occurrence of incident fracture in postmenopausal women. This assessment may play an important role in identifying women at high risk of fracture who could not be adequately detected by BMD measurement alone, to benefit from a therapeutic intervention. © 2017 American Society for Bone and Mineral Research.

KEY WORDS: BONE HR-pQCT; ANALYSIS/QUANTITATION OF BONE; OSTEOPOROSIS; DISEASES AND DISORDERS OF/RELATED TO BONE; FRACTURE RISK ASSESSMENT; BONE MICROARCHITECTURE; POST-MENOPAUSAL WOMEN; EPIDEMIOLOGY

Introduction

High-resolution peripheral computed tomography (HR-pQCT) enables a noninvasive three-dimensional (3D) evaluation of bone microarchitecture in vivo. It distinguishes the cortical and trabecular compartments of the distal radius and tibia. HR-pQCT confers significant advantages over two-dimensional (2D) measurements based on dual-energy X-ray absorptiometry (DXA), by providing assessment not only of BMD, but also of bone structure and strength, both in the trabecular and cortical compartments. Several cross-sectional studies have shown that impairment of bone microarchitecture was associated with prevalent fracture. In postmenopausal women, lower volumetric bone density (vBMD), cortical thickness, and trabecular number, and greater heterogeneity of the trabecular network were associated with previous wrist,[1–3] hip,[3] vertebral,[4,5] and all fragility fractures.[6] Those decreases were greater at the radius for trabecular parameters (number, separation, and heterogeneity) whereas cortical thickness was diminished only at the distal tibia or at both sites.[3,7] In those studies, the alterations of bone microarchitecture were partially independent of areal bone density assessed by DXA. A recent multicentric study conducted in 1379 white postmenopausal women from five centers worldwide showed, by combining data of all centers, that women with prevalent fracture had significantly lower total, trabecular, and cortical vBMD, lower trabecular number, and thinner cortices than women without fracture after adjustment for covariates, with similar results at both bone sites.[8] The major limitation of previous cross-sectional studies is that HR-pQCT measurements were done retrospectively after the fractures were sustained. Until now, the independent contribution of cortical and trabecular architecture to the risk of fracture has not been evaluated prospectively in women.

Received in original form September 20, 2016; revised form January 19, 2017; accepted February 4, 2017. Accepted manuscript online March 9, 2016.
Address correspondence to: Elisabeth Sornay-Rendu, MD, Hôpital Edouard Herriot, Pavillon F, INSERM UMR 1033, 69437 Lyon Cedex 03, France.
E-mail: elisabeth.rendu@inserm.fr
*ESR and SB contributed equally to this work.
Additional Supporting Information may be found in the online version of this article.
Journal of Bone and Mineral Research, Vol. 32, No. 6, June 2017, pp 1243–1251
DOI: 10.1002/jbmr.3105

Besides bone microarchitecture measurement, the high resolution of HR-pQCT permits to estimate bone strength using finite element analysis (FEA), incorporating both material and architectural components of bone strength. This estimated bone strength is highly correlated with direct measurement of bone strength by mechanical testing.[9] Thus, several cross-sectional studies have shown that bone stiffness evaluated with FEA discriminated postmenopausal women with and without prevalent low-trauma fracture.[1,2,7,10–12] So, prospective data are needed to confirm the prediction of fracture by estimated bone strength. Furthermore, cortical porosity, which is the result of bone resorption on the endocortical surface and on the surface of Haversian canals, could be a significant contributor of bone strength.[13,14] Its assessment has been added to microstructural features accessible with HR-pQCT[15–17] and several cross-sectional studies confirmed it increases with age in women, particularly after menopause.[18–20] Nevertheless, the role of cortical porosity to predict incident fracture remains to be established.

The aim of our study was to prospectively investigate the prediction of fragility fracture by bone microarchitecture and FEA-estimated bone strength assessed by HR-pQCT, in French postmenopausal women.

Subjects and Methods

Subjects

All subjects were participants of the Os des Femmes de Lyon (OFELY) cohort, which is a prospective study of the determinants of bone loss in 1039 volunteer women, started in February 1992.[21,22] Our study focused on the 589 postmenopausal white women, aged 68 ± 9 years, who had a bone microarchitecture measurement between years 2006 and 2008 (ie, at their 14th follow-up visit, corresponding to the first visit with bone microarchitecture assessment). The protocol was approved by an independent ethics committee and all patients gave written informed consent prior to participation.

Clinical assessment

At the same visit, all women completed a written health questionnaire,[22] including current smoking, menopausal status, medication use, falls during the past 12 months, and occurrence of radiologically confirmed low-trauma fractures. The 10-year probabilities of a major fracture (hip, clinical spine, humerus, or wrist fracture) and hip fracture were calculated with the Fracture Risk Assessment Tool (FRAX) algorithm.[23] Data related to the use of osteoporosis-related drugs (bisphosphonates, hormone replacement therapy, selective estrogen-receptor modulators, tibolone) and bone loss–inducing therapy (corticosteroids, aromatase inhibitors) were considered in this analysis if the duration of treatment was more than 1 year (3 months for corticosteroids) at the time (or ended within 6 months before) of bone microarchitecture evaluation. Height and body weight were recorded.

Fracture evaluation

For the present analysis, prevalent fragility fractures were all those that occurred since the inclusion in the study, in addition to the fragility fractures of the wrist, humerus, vertebrae, or hip that occurred before the inclusion in the study and after the age of 40 years. Incident nonvertebral and clinical vertebral fractures were annually registered between the observation period (2006 and 2008) and the last follow-up visit (2015–2016) by questionnaire and were all confirmed by radiographs or surgical reports. Only fragility fractures resulting from low-trauma (ie, those occurring after falls from standing height or less) were taken into account and we excluded fractures of the head, toes, and fingers. Vertebral fractures that did not reach clinical attention were identified according to the semiquantitative method of Genant and colleagues[24] by a trained rheumatologist (ESR), on lateral X-ray films of the thoracic and the lumbar spine performed at the 14th and 18th follow-up (ie, at baseline and 4 years later for the present study) and on DXA, using vertebral fracture assessment (VFA) software (Hologic Discovery densitometer, Hologic, Inc., Bedford, MA), at the 20th, 22th, and 24th follow-up (ie, 6, 8, and 10 years after baseline). Both clinical and morphometric incident vertebral fractures were taken into account in the analyses, except for the analysis of major fractures that include only clinical spine fractures.

Measurement of BMD and bone microarchitecture

Lumbar spine and total hip areal bone mineral densities (aBMD, g/cm^2) were measured using DXA (QDR 4500; Hologic, Bedford, MA, USA). *T*-scores were calculated from the Hologic France reference values. Using the WHO classification,[18–20] these women were classified as normal (*T*-score > -1), osteopenic ($-1 \geq$ *T*-score > -2.5), or osteoporotic (*T*-score ≤ -2.5) based on the lower values of their aBMD measurements at the lumbar spine or total hip. The *T*-score at the femoral neck was calculated from the National Health and Nutrition Examination Survey III (NHANES III) reference values and was used to calculate the FRAX probabilities.

Volumetric density and bone microarchitecture were assessed at the nondominant distal radius and tibia by HR-pQCT (XtremeCT; Scanco Medical AG, Brüttisellen, Switzerland) according to the manufacturer's standard in vivo acquisition protocol (60 kVp, 900 mA, matrix size of 1536×1536).[25,26] The measurement region was manually defined by the operator and consisted of an approximately 9 mm length of bone located 9.5 to 18.5 mm and 22.5 to 31.5 mm proximal to the endplate for the radius and tibia, respectively. Methods used to process the CT data have been described in detail.[26] A recent automatic segmentation script was used to differentiate cortical bone from trabecular bone,[17] which permitted the assessment of extended cortical parameters such as cortical porosity. This method is based on the generation of periosteal and endosteal contours that were subsequently visually validated. HR-pQCT outcomes parameters included: total (Tt), cortical (Ct), and trabecular (Tb) volumetric bone density (Tt.BMD, Ct.BMD, and Tb.BMD, mg/cm^3) and area (Tt.Ar, Ct.Ar, and Tb.Ar, mm^2); cortical thickness (Ct.Th, μm) measured by direct 3D method disregarding the presence of pores and porosity (Ct.Po, %); trabecular number (Tb.N, mm^{-1}), and intraindividual distribution of separation (Tb.Sp.SD, mm). Non-metric trabecular indices were also assessed: the structural model index (SMI, no unit) related to the rod-like or plate-like topology of the trabecular network, and the connectivity density (Conn.D, no unit). HR-pQCT quality scans were reviewed by an experimented operator, and graded into five classes from 0 for perfect scans to 4 for the poorest scans.[27] Scans with poor quality, ie, grade 4, were excluded from the analyses.

FEA

Finite element models of the radius and tibia were created directly from the segmented HR-pQCT images using software delivered with the HR-pQCT device (IPL; Scanco Medical AG). A voxel-conversion procedure was used to convert each voxel of bone tissue into an equally sized brick element (~2 million elements for the radius, 5 million elements for the tibia).[28] Material properties were chosen isotropic and elastic. Cortical and trabecular bone elements were assigned a Young's modulus of 20 and 17 GPa, respectively.[29] All elements were specified a Poisson's ratio of 0.3. A compression test was simulated in which a load in the longitudinal direction was applied at one end while the other end was fully constrained, as described.[30] To reproduce Pistoia's criterion where failure is expected when 2% of the bone tissue is strained beyond a critical limit of 7000 μstrain (with a Young's modulus of 10 GPa), we had to set the critical strain to 3500 μstrain.[1]

FEA outcomes parameters included failure load (N) and stiffness (kN/mm). All micro–finite element (μFE) analyses were done using the FE solver integrated in the IPL software v1.13 (Scanco Medical AG).

Statistical analysis

The baseline characteristics of the women were presented as mean ± SD for continuous variables and number (percentage) of patients for categorical variables. Differences between groups were expressed in percentage from women without incident fracture. Student's *t* test, Wilcoxon signed-rank test, and chi-square test were used to compare baseline characteristics between women with and without incident fractures, depending on the distribution of the variables. Cox proportional hazards models based on time to the first fragility fracture were used to calculate hazard ratios with their 95% confidence interval (HR; 95% CI), to estimate the fracture risk prediction for a quartile change of bone parameter. All models were first adjusted for age and multivariable models included variables that remained significant after adjusting for age. All statistical analyses were performed using Stata 12 (StataCorp LP, College Station, TX, USA).

Results

Among the 589 postmenopausal women, 135 women sustained at least one incident fragility fracture (Fx), including 81 women with a major osteoporotic (MOP) Fx; ie, clinical spine ($n = 27$), distal forearm ($n = 31$), hip ($n = 15$), proximal humerus ($n = 8$), and 54 women with other types of Fx (morphometric vertebral Fx [$n = 12$], ankle [$n = 12$], lower leg [$n = 14$], pelvis [$n = 2$], upper leg [$n = 7$], clavicle [$n = 1$], rib [$n = 5$], and sternum [$n = 1$]), during a median [IQ] follow-up of 9.4 [1.0] years. Incident fractures occurred over an average of 4.9 ± 3.0 years (from 2 months to 10.3 years) from baseline.

All women had at least one valid HR-pQCT scan (radius and/or tibia). There were 18 radius and 12 tibia scans excluded (poor scan quality [$n = 22$, 73%], fracture on both sides). Consequently, there were 571 (97%) radius scans and 577 (98%) tibia scans used in this study. Hip and lumbar spine DXA measurements were obtained in 584 and 587 women, respectively.

As shown in Table 1, at the time of baseline DXA and HR-pQCT scans, women with incident fractures were significantly older. After adjusting for age, prior Fx, current smoking, and use of osteoporosis-related drugs, falls in the last year were more frequent and aBMD was lower in women with incident fractures compared with women without fracture.

Women who sustained incident Fx had significant impairment of most of microarchitecture parameters and estimated bone

Table 1. Characteristics of Women at Baseline With and Without Incident Fragility Fx: All Fx or MOP Fx

	Non-Fx ($n = 454$)	All Fx ($n = 135$)	Age-adjusted *p*	MOP Fx ($n = 81$)	Age-adjusted *p*
Age (years)	67.4 ± 8.5	70.6 ± 8.7[a]	–	72.1 ± 8.7[a]	–
Weight (kg)	62 ± 11	62 ± 12	0.8	61 ± 12	0.4
Height (cm)	158 ± 6	158 ± 6	0.2	158 ± 6	0.2
BMI (kg/m^2)	24.9 ± 4.2	24.7 ± 4.7	0.4	24.3 ± 4.8[c]	0.1
Menopausal age (years)	50.4 ± 3.9	51.1 ± 3.7	0.1	50.9 ± 4.0	0.4
Falls in the past year	0.51 ± 0.96	0.75 ± 1.38[c]	0.03	0.76 ± 1.15	0.06
Prior Fx, *n* (%)	79 (17)	43 (32)[a]	0.01	27 (33)[b]	0.08
Current smokers, *n* (%)	23 (5)	14 (10)[c]	0.002	8 (10)	0.007
Osteoporotic-related drugs, *n* (%)[d]	116 (26)	47 (35)[c]	0.009	31 (38)	0.003
Bone loss–inducing therapy, *n* (%)[e]	12 (3)	3 (2)	0.9	2 (2)	0.6
FRAX major without BMD	10.0 ± 9.2	13.9 ± 10.8[a]	–	15.8 ± 12.2[a]	–
FRAX major with BMD	7.5 ± 6.7	10.2 ± 7.3[a]	–	11.2 ± 7.9[a]	–
FRAX hip without BMD	4.3 ± 6.8	7.1 ± 8.7[a]	–	8.6 ± 9.9[a]	–
FRAX major with BMD	2.3 ± 4.4	3.9 ± 5.1[a]	–	4.5 ± 5.3[a]	–
Lumbar spine aBMD (g/cm^2)	0.907 ± 0.144	0.860 ± 0.139[b]	0.002	0.848 ± 0.136[b]	0.001
Lumbar spine *T*-score	−0.84 ± 1.27	−1.26 ± 1.23[b]	0.002	−1.37 ± 1.20[b]	0.001
Total hip aBMD (g/cm^2)	0.847 ± 0.114	0.803 ± 0.118[a]	0.01	0.788 ± 0.122[a]	0.01
Total hip *T*-score	−0.74 ± 1.10	−1.17 ± 1.14[a]	0.01	−1.31 ± 1.18[a]	0.01

Values are mean ± SD or *n* (%), as indicated.
Fx = fracture; MOP = major osteoporotic.
[a] $p < 0.001$ versus non-Fx.
[b] $p < 0.01$ versus non-Fx.
[c] $p < 0.05$ versus non-Fx.
[d] Bisphosphonates, hormone replacement therapy, selective estrogen receptor modulator, tibolone.
[e] Aromatase inhibitors, corticosteroids.

strength at both sites with greater differences for MOP incidence Fx. After adjusting for age, total and Tb vBMD at both sites, cortical parameters (area and thickness at the radius, area and vBMD at the tibia), trabecular number (Tb.N), SMI, connectivity density, stiffness, and estimated failure load at both sites remained significantly altered in women with incident fracture (Table 2).

At the radius, each quartile decrease of baseline values of Tt.BMD, Tb.BMD, Ct.Ar, Tb.N, Tb.Sp.SD, SMI, Conn.D, stiffness, and estimated failure load was associated with a significant increase (decrease for Tb.Sp.SD and SMI) of the risk of all fragility fractures after adjusting for age ($p \leq 0.01$). Adding prior Fx, current smoking, falls in the past year, and use of osteoporosis-related drugs to the model, the association with the risk of fracture remained significant for all these microarchitectural parameters ($p \leq 0.02$). After further addition of total hip BMD to the multivariate model, the association remained significant for Tb.BMD, Tb.N, Tb.Sp.SD, Conn.D, stiffness, and failure load (Table 3 and Supplemental Table 1). Similar results were obtained for MOP Fx in the two first models (data not shown). After further adjustment for total hip BMD, the association remained significant for Tt.vBMD, Tb.vBMD, Tb.N, Tb.Sp.SD, Conn.D, and stiffness (Fig. 1). Similar results were obtained with the osteoporotic threshold. Without adding microarchitecture in the model, and using normal BMD as the reference group, the multivariate-adjusted HR (95% CI) for women with osteoporosis ($n = 77$) was 2.77 (95% CI, 1.67 to 4.61) for all Fx and 3.79 (95% CI, 1.93 to 7.45) for MOP Fx, $p < 0.0001$ for both. For women with osteopenia ($n = 295$), the multivariate-adjusted HR (95% CI) was 0.93 (95% CI, 0.61 to 1.41) for all Fx and 1.07 (95% CI, 0.60 to 1.91) for MOP Fx. For women with both osteoporosis and low levels of Tb.N (first quartile) ($n = 46$), the multivariate-adjusted HR increased to 3.39 (95% CI, 2.05 to 5.61) for all Fx and 4.57 (95% CI, 2.44 to 8.56) for MOP Fx, $p < 0.0001$ for both.

At the distal tibia, each quartile decrease of baseline values of Tt.vBMD, Tb.vBMD, Ct.Ar, Tb.N, Tb.Sp.SD, SMI, Conn.D, stiffness, and estimated failure load were associated with a significant increase (decrease for Tb.Sp.SD) of the risk of fracture after adjusting for age ($p \leq 0.04$). In the multivariate model, the association with the risk of fracture remained significant for those parameters except for Ct.Ar and SMI. After adding total hip BMD to the multivariate model, the association with the risk of fracture remained significant only for failure load (Table 3 and Supplemental Table 1). For MOP Fx, in the multivariate model including total hip BMD, the association remained significant for Tt.BMD, stiffness, and estimated failure load (Fig. 1). For women with both osteoporosis and low levels of estimated failure load (first quartile) ($n = 54$), the multivariate-adjusted HR was 2.16 (95% CI, 1.31 to 3.56) for all Fx and 2.34 (95% CI, 1.26 to 4.34) for MOP Fx, $p < 0.0001$ for both.

Finally, impairment of bone microarchitecture was still significantly associated with an increase of the risk of Fx after adjusting for FRAX probabilities (Table 3).

Discussion

In this first epidemiological prospective study of fracture risk assessed with HR-pQCT, we found that in French postmenopausal women from the OFELY cohort, prospectively followed during 9 years, impairment of bone microarchitecture at both radius and tibia predict the risk of fragility fracture. This effect was observed for all types of fractures.

As previously shown in cross-sectional studies, we found differences according to the site of measurement. In the same cohort, we previously observed greater impairment of trabecular parameters at the distal radius as compared to tibia.[6,11] These abnormalities were also more strongly associated with the risk of incident fracture. The better prediction with the radius measures may stem from the fact that the trabecular parameters were better predictors of fracture than cortical ones. The poor association with incident fracture of cortical parameters and of a more cortical site like the tibia remain to be explained. This may be because of the relatively young age of our postmenopausal group of women, who are less exposed to fractures related to impairment of the cortical bone, such as hip fracture. Of note, a distal site such as the radius was associated with fracture at distant sites, including the spine.

In one study conducted in postmenopausal women (30 with prevalent vertebral fracture, 73 with nonvertebral fracture, and 120 controls), vertebral fractures appeared to be more strongly associated with poor bone quality compared with nonvertebral fractures at the distal tibia, with lower total and trabecular volumetric densities, cortical thickness, and trabecular number, and greater trabecular separation and network heterogeneity, whereas no difference was observed at the radius.[31] In our prospective study, we did not observe significant differences of microarchitecture parameters between individuals with vertebral ($n = 38$) and nonvertebral fractures ($n = 97$) at both the distal radius and tibia (data not shown).

Our prospective study confirmed previous cross-sectional studies showing that bone structure and strength contribute to low-trauma fracture risk independently of aBMD.[1,2,4–6,11,12] In the same cohort, we have previously shown that both microarchitecture and bone mechanical properties assessed by FEA based on HR-pQCT images were associated with fragility fracture of the wrist[1] and of all sites.[11] Using principal component analysis, we found that FEA-derived bone strength characterized a large part of biomechanical properties of the distal radius[1] and tibia.[11]

In a case-control study, Nishiyama and colleagues[12] showed, by using a machine learning technique based on support vector machines (SVM) model, that models based on HR-pQCT measurements of bone microarchitecture and estimates of bone strength performed better than DXA-derived aBMD at classifying postmenopausal women with and without prior low-trauma fractures and more particularly forearm fractures. In that study, the model including only FEA parameters had similar performance than a model including HR-pQCT microarchitecture parameters, DXA, and FEA parameters, suggesting that the FEA measurements provide a good evaluation of bone quality. In our study, at the tibia site, estimated failure load and stiffness were the only parameters that remained significantly associated with the risk of all incident fracture after adjusting for osteoporosis defined by aBMD. In contrast, at the distal radius, both microarchitecture parameters and estimated bone strength contributed to the increased risk of incident fracture independently of osteoporosis defined by aBMD. That confirms the importance of the role of estimated bone strength on the risk of fracture especially on a weight-bearing site. In a case-control study, Stein and colleagues[7] have shown a reduction of stiffness evaluated by FEA in fractured patients that was more marked at the radius (41% to 44%) than at the tibia (15% to 20%). Conversely, in a previous cross-sectional analysis from the OFELY cohort,[11] the reduction of stiffness and estimated failure load were of the same order of magnitude at both sites (11% to 13%)

Table 2. Microarchitecture and Estimated Bone Strength of Women at Baseline With and Without Incident Fragility Fx: All Fx or MOP Fx

	Non-Fx ($n = 454$)	All Fx ($n = 135$)	Difference (%)	Age-adjusted p	MOP Fx ($n = 81$)	Difference (%)	Age-adjusted p
Radius							
Tt.Ar (mm^2)	256 ± 42	256 ± 46	0	0.9	258 ± 47	1	0.8
Ct.Ar (mm^2)	42.1 ± 8.9	38.9 ± 8.5[a]	−7.6	0.02	37.6 ± 8.1[a]	−11	0.01
Tb.Ar (mm^2)	205 ± 43	208 ± 46	1	0.6	211 ± 47	3	0.5
Tt.BMD (mg/cm^3)	279 ± 68	249 ± 63[a]	−11	0.002	237 ± 59[a]	−15	0.0001
Ct.BMD (mg/cm^3)	803 ± 80	777 ± 77[b]	−3	0.08	767 ± 77[a]	−4	0.07
Tb.BMD (mg/cm^3)	143 ± 41	123 ± 39[a]	−14	0.0001	114 ± 36[a]	−20	0.0001
Ct.Th (mm)	0.796 ± 0.169	0.741 ± 0.160[b]	−7	0.03	0.717 ± 0.153[a]	−10	0.02
Ct.Po (%)	2.81 ± 1.90	3.02 ± 1.93	7	0.9	3.00 ± 1.96	7	0.8
Tb.N (1/mm)	1.57 ± 0.32	1.43 ± 0.31[a]	−9	0.002	1.38 ± 0.33[a]	−12	0.001
Tb.Sp.SD (mm)	0.329 ± 0.231	0.377 ± 0.202[a]	15	0.5	0.404 ± 0.219[a]	23	0.4
SMI	2.22 ± 0.34	2.34 ± 0.32[b]	5	0.007	2.40 ± 0.29[a]	8	0.001
Conn.D	2.74 ± 0.89	2.34 ± 0.89[a]	−15	0.001	2.16 ± 0.89[a]	−21	0.0001
Stiffness (kN/mm)	119 ± 27	107 ± 24[a]	−10	0.001	102 ± 21[a]	−14	0.0001
Failure load (N)	2801 ± 621	2523 ± 563[a]	−10	0.001	2417 ± 481[a]	−14	0.0001
Tibia							
Tt.Ar (mm^2)	661 ± 96	673 ± 115[b]	2	0.3	675 ± 111[a]	2	0.4
Ct.Ar (mm^2)	99.2 ± 15.7	94.5 ± 18.0[b]	−5	0.04	91.7 ± 18.6[a]	−8	0.006
Tb.Ar (mm^2)	549 ± 98	565 ± 119	3	0.2	570 ± 117	4	0.2
Tt.BMD (mg/cm^3)	254 ± 53	229 ± 54[a]	−10	0.001	219 ± 52[a]	−14	0.0001
Ct.BMD (mg/cm^3)	746 ± 100	707 ± 102[a]	−5	0.04	691 ± 101[a]	−7	0.04
Tb.BMD (mg/cm^3)	150 ± 38	134 ± 36[a]	−11	0.0001	129 ± 35[a]	−14	0.0001
Ct.Th (mm)	1.119 ± 0.213	1.136 ± 0.239	2	0.3	1.133 ± 0.232	1	0.4
Ct.Po (%)	14.3 ± 7.4	16.8 ± 7.9[b]	17	0.2	17.5 ± 8.0[a]	22	0.3
Tb.N (1/mm)	1.52 ± 0.29	1.40 ± 0.34[a]	−8	0.0001	1.37 ± 0.36[a]	−10	0.001
Tb.Sp.SD (mm)	0.322 ± 0.2022	0.433 ± 0.408[a]	34	0.002	0.450 ± 0.385[a]	40	0.002
SMI	1.80 ± 0.36	1.89 ± 0.36[c]	5	0.02	1.94 ± 0.34[b]	8	0.005
Conn.D	2.76 ± 0.77	2.48 ± 0.76[a]	−10	0.002	2.42 ± 0.80[a]	−12	0.003
Stiffness (kN/mm)	328 ± 59	299 ± 58[a]	−9	0.001	286 ± 53[a]	−13	0.0001
Failure load (N)	7764 ± 1346	7123 ± 1320[a]	−8	0.001	6830 ± 1197[a]	−12	0.0001

Values are mean ± SD.

Fx = fracture; MOP = major osteoporotic.

[a] $p < 0.001$ versus non-Fx.

[b] $p < 0.01$ versus non-Fx.

[c] $p < 0.05$ versus non-Fx.

Table 3. Association Between Bone Microarchitecture Parameters and the Risk of All Incident Fragility Fracture

	Unit	Age-adjusted HR (95% CI)	*p*	Adjusted HR (95% CI)[a]	p^a	Adjusted HR (95% CI)[b]	p^b	Adjusted HR (95% CI)[c]	p^c
Radius									
Tt.Ar	↓ Quartile	1.02 (0.87–1.19)	0.77	1.01 (0.86–1.19)	0.88	1.02 (0.87–1.19)	0.82	1.05 (0.89–1.23)	0.56
Ct.Ar	↓ Quartile	1.25 (1.05–1.49)	**0.01**	1.25 (1.04–1.49)	**0.02**	1.15 (0.94–1.39)	0.18	1.28 (1.08–1.54)	**0.007**
Tb.Ar	↓ Quartile	1.01 (0.86–1.19)	0.86	1.01 (0.85–1.17)	0.99	0.98 (0.87–1.19)	0.81	1.03 (0.88–1.20)	0.72
Tt.BMD	↓ Quartile	1.33 (1.11–1.58)	**0.002**	1.29 (1.07–1.56)	**0.006**	1.20 (0.99–1.47)	0.06	1.35 (1.11–1.61)	**0.002**
Ct.BMD	↓ Quartile	1.14 (0.95–1.36)	0.14	1.14 (0.96–1.38)	0.13	1.08 (0.89–1.30)	0.43	1.20 (1.01–1.49)	**0.04**
Tb.BMD	↓ Quartile	1.49 (1.25–1.75)	<**0.0001**	1.44 (1.20–1.72)	<**0.0001**	1.39 (1.15–1.69)	**0.001**	1.49 (1.25–1.82)	<**0.0001**
Ct.Th	↓ Quartile	1.17 (0.99–1.38)	0.06	1.16 (0.98–1.36)	0.09	1.08 (0.89–1.28)	0.47	1.18 (0.99–1.41)	0.06
Ct.Po	↓ Quartile	1.00 (0.85–1.17)	0.99	0.99 (0.83–1.16)	0.87	0.98 (0.83–1.16)	0.84	0.93 (0.79–1.10)	0.40
Tb.N	↓ Quartile	1.44 (1.21–1.69)	<**0.0001**	1.38 (1.14–1.66)	<**0.0001**	1.32 (1.08–1.61)	**0.006**	1.43 (1.19–1.72)	<**0.0001**
Tb.Sp.SD	↓ Quartile	0.69 (0.58–0.81)	<**0.0001**	0.71 (0.59–0.86)	<**0.0001**	0.76 (0.63–0.92)	**0.005**	0.70 (0.58–0.84)	<**0.0001**
SMI	↓ Quartile	0.78 (0.67–0.92)	**0.004**	0.82 (0.69–0.97)	**0.02**	0.87 (0.72–1.03)	0.11	0.81 (0.68–0.96)	**0.02**
Conn.D	↓ Quartile	1.44 (1.21–1.72)	<**0.0001**	1.36 (1.13–1.63)	**0.001**	1.49 (1.05–1.30)	**0.01**	1.39 (1.15–1.67)	<**0.0001**
Stiffness	↓ Quartile	1.38 (1.16–1.63)	<**0.0001**	1.35 (1.12–1.61)	**0.002**	1.27 (1.03–1.55)	**0.02**	1.39 (1.16–1.69)	<**0.0001**
Failure load	↓ Quartile	1.35 (1.13–1.61)	**0.001**	1.33 (1.09–1.58)	**0.003**	1.23 (1.01–1.52)	**0.04**	1.37 (1.14–1.64)	**0.001**
Tibia									
Tt.Ar	↓ Quartile	0.92 (0.79–1.08)	0.34	1.01 (0.86–1.19)	0.35	0.93 (0.80–1.10)	0.44	0.95 (0.81–1.11)	0.55
Ct.Ar	↓ Quartile	1.21 (1.04–1.42)	**0.01**	1.25 (1.04–1.49)	0.10	1.08 (0.91–1.28)	0.40	1.16 (0.97–1.37)	0.10
Tb.Ar	↓ Quartile	0.90 (0.78–1.06)	0.23	1.01 (0.85–1.17)	0.27	0.93 (0.79–1.09)	0.35	0.93 (0.79–1.09)	0.36
Tt.BMD	↓ Quartile	1.38 (1.16–1.63)	<**0.0001**	1.29 (1.07–1.56)	**0.01**	1.16 (0.94–1.45)	0.15	1.32 (1.10–1.59)	**0.003**
Ct.BMD	↓ Quartile	1.19 (0.99–1.44)	0.07	1.14 (0.96–1.38)	0.14	1.06 (0.86–1.30)	0.57	1.23 (1.03–1.47)	**0.03**
Tb.BMD	↓ Quartile	1.33 (1.13–1.56)	<**0.0001**	1.44 (1.20–1.72)	**0.02**	1.16 (0.96–1.41)	0.11	1.28 (1.08–1.54)	**0.005**
Ct.Th	↓ Quartile	0.96 (0.82–1.12)	0.63	1.16 (0.98–1.36)	0.74	0.97 (0.83–1.14)	0.71	1.01 (0.86–1.19)	0.89
Ct.Po	↓ Quartile	0.89 (0.74–1.07)	0.23	0.99 (0.83–1.16)	0.24	0.96 (0.79–1.18)	0.70	0.85 (0.72–1.02)	0.09
Tb.N	↓ Quartile	1.25 (1.07–1.47)	**0.005**	1.38 (1.14–1.66)	**0.045**	1.10 (0.93–1.32)	0.28	1.19 (1.01–1.41)	**0.04**
Tb.Sp.SD	↓ Quartile	0.77 (0.66–0.90)	**0.002**	0.71 (0.59–0.86)	**0.02**	0.87 (0.73–1.04)	0.14	0.80 (0.68–0.94)	**0.009**
SMI	↓ Quartile	0.84 (0.72–0.99)	**0.04**	0.82 (0.69–0.97)	0.22	0.95 (0.81–1.14)	0.62	0.89 (0.76–1.05)	0.19
Conn.D	↓ Quartile	1.25 (1.06–1.47)	**0.006**	1.36 (1.13–1.63)	**0.045**	1.11 (0.93–1.33)	0.25	1.22 (1.03–1.45)	**0.02**
Stiffness	↓ Quartile	1.44 (1.21–1.72)	<**0.0001**	1.35 (1.12–1.61)	<**0.0001**	1.34 (1.08–1.66)	0.009	1.45 (1.20–1.75)	<**0.0001**
Failure load	↓ Quartile	1.44 (1.21–1.72)	<**0.0001**	1.33 (1.09–1.58)	**0.001**	1.31 (1.05–1.63)	0.02	1.45 (1.19–1.72)	<**0.0001**

[a]Adjusted HR for age, current smoking, falls in the past year, prior Fx, use of osteoporosis-related drugs.
[b]Adjusted HR for age, current smoking, falls in the past year, prior Fx, use of osteoporosis-related drugs, and total hip BMD.
[c]Adjusted HR for FRAX major with BMD, falls in the past year, use of osteoporosis-related drugs.

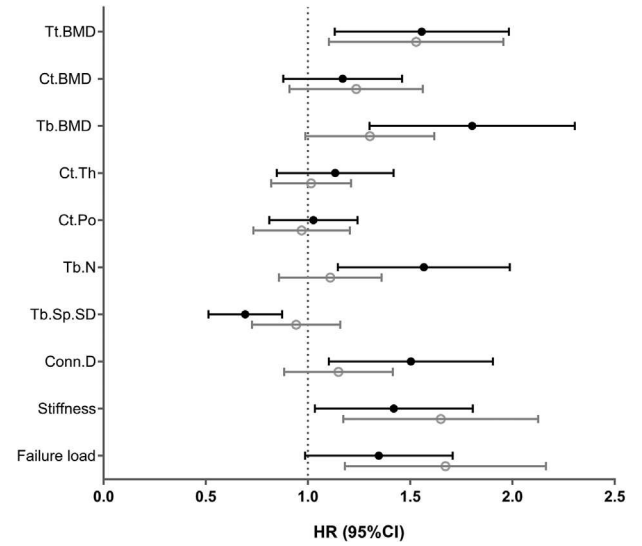

Fig. 1. Association between bone microarchitecture at the distal radius (black lines) and tibia (gray lines) and the risk of incident MOP fracture. Hazard ratios (95% CI) per one-quartile decrease of bone parameter are adjusted for age, current smoking, falls in the past year, prior Fx, osteoporosis-related drug use, and total hip BMD.

in women with prevalent fragility fracture[11] and we found similar differences in the present prospective study with reduction of stiffness and estimated failure load at both sites of 8% to 10% in women with incident fragility fracture, at all sites. Different methods assessing stiffness by FEA could explain some discrepancies. Indeed, the evaluation of stiffness was limited to the trabecular compartment in the study of Stein and colleagues,[7] contrasting with the analysis of both trabecular and cortical compartments in other studies.

Despite the impairment of cortical bone at baseline among women who will sustain incident fracture (lower cortical area and thickness at both sites), we did not find any difference for cortical porosity. No cross-sectional study using the same recent automatic threshold-based segmentation method from HR-pQCT found any association between cortical porosity and prevalent fracture in postmenopausal women.[5,10,12] Nevertheless, we previously found in a cross-sectional analysis from the OFELY cohort that cortical porosity was markedly impaired with age, in association with decreased failure load, especially at the tibia in postmenopausal women. At this site, cortical porosity increased from a median of 4% in premenopausal women to 14% in postmenopausal women.[19] Comparatively, in the present prospective study limited to postmenopausal women, the difference in cortical porosity between women with and without incident fracture was much lower (17% and 14%, respectively) and was not independent of age. Moreover in the present study, we did not find a significant association between cortical porosity with further risk of fracture. Using another density-based method of segmentation, Bala and colleagues[32] found an association between cortical porosity and prevalent forearm fractures in postmenopausal women with osteopenia. That study used a new algorithm (StrAx1.0) that bases segmentation and cortical porosity measurement on a density profile analysis across the cortex, identifying a transitional zone between the cortical and trabecular compartments.[33] Using the same method, Bjørnerem and colleagues[34] showed, in a twin study of 345 women aged 40 to 61 years, including 26% postmenopausal women, and 93 women with a history of fracture during childhood or adulthood, a positive association between cortical porosity at the distal tibia and fibula (not at the radius) and the risk of fracture after adjustment for age, height, and weight. They found much higher values of porosity compared to our study (almost 50% at the distal radius and 60% at the distal tibia contrasting to less than 20% at both sites in our study) that would suggest the incorporation of some trabecular bone with the StrAx method. This likely stems from the fact that the StrAx so-called transitional zone corresponds to an area of trabecularized endosteal cortical bone that is recognized as trabecular bone by the standard analysis. Thus, the discrepancies between studies may be explained by the different methods of segmentation of the cortical and trabecular compartments, the variability in the localization of the analyzed voxels of interest and the different characteristics of the women (age, menopausal status, bone status according to aBMD classification). Segmentation between the cortical and trabecular compartments is challenging because there is rarely a precise border between them. Despite the fact that HR-pQCT (XTreme CT) has been the highest resolution in vivo scanner available for human bone measurements, the 82-μm voxel size is close to the size of trabeculae. In addition, direct quantification of porosity by HR-pQCT is limited to relatively large Haversian canals. Moreover, the porosity gradient along the cortical thickness due to the trabecularization of the cortex with aging is another source of difficulty to delineate both compartments.[33,35,36] Furthermore, a recent study showed that during both growth and aging, changes in pore network microarchitecture—that reflects activity and balance of remodeling upon canal surfaces—contribute to bone stiffness independently of the changes in the void volume fraction.[37]

Our study has strengths and limitations. The OFELY study is a population-based cohort study, and all fragility fractures were prospectively assessed and radiographically confirmed. In addition to bone microarchitecture measurements, aBMD and clinical risk factors of fracture were collected at baseline. The information of incident fracture was obtained for most of women, because only 36 (7.9%) nonfractured women were lost before the end of the 9 years of observation. In contrast to previous cross-sectional studies, this prospective study permitted to reflect bone microarchitecture and bone strength by FEA at the time of the fracture.

One of the limitations is the relatively small number of incident fractures, including few hip fractures because these women are relatively young. Thus, the sample size was not sufficient to analyze bone microarchitecture alterations specifically in women with osteopenia. Moreover, women were French community-dwelling white volunteers, and our findings may not be generalized to other populations. In addition, among the trabecular parameters significantly associated with the risk of fracture, SMI and Conn.D have been less validated than metric indices with HR-pQCT. Nevertheless, a cross-sectional study from the OFELY cohort showed an increase of SMI with age and a contribution of SMI to predict failure load in both premenopausal and postmenopausal women.[19] In the cohort from Mayo Clinic, these two parameters did not differ significantly both in men and women who were aBMD-matched.[20] In addition, SMI has been associated with stiffness in another cross-sectional analysis from OFELY.[38] Moreover, the impact of spatial resolution on the non-metric indices (ie, SMI, ConnD, and

degree of anisotropy) to the in vivo imaging of trabecular bone structure has been reported.[27] If the authors clearly showed that those indices were affected by low spatial resolution of CT images, SMI and ConnD obtained from μCT at 16 μm and HR-pQCT at 82 μm were highly correlated ($r = 0.95$ and 0.87, respectively).

In conclusion, in this first epidemiological prospective study of fracture risk with HR-pQCT, we found that in French postmenopausal women from the OFELY cohort, prospectively followed during 9 years, impairment of bone microarchitecture at both radius and tibia predicts the risk of all fragility fracture. Their assessment may play an important role in identifying women at high risk of fracture who could not be adequately detected by BMD measurement alone, and who may benefit from a therapeutic intervention.

Disclosures

All authors state that they have no conflicts of interest.

Acknowledgments

We thank A. Bourgeaud-Lignot, S. Ailloud, and D. Foesser for valuable technical assistance.

Authors' roles: Study design: ESR, SB, and RC. Study conduct: ESR, SB, FD, and RC. Data collection: ESR, SB, and FD. Data analysis: ESR and SB. Data interpretation: ESR, SB, and RC. Drafting manuscript: ESR and SB. Revising manuscript content: ESR, SB, and RC. Approving final version of manuscript: ESR, SB, FD, and RC. ESR takes responsibility for the integrity of the data analysis.

References

1. Boutroy S, van Rietbergen B, Sornay-Rendu E, Munoz F, Bouxsein ML, Delmas PD. Finite element analysis based on in vivo HR-pQCT Images of the distal radius is associated with wrist fracture in postmenopausal women. J Bone Miner Res. 2008;23:392–9.
2. Melton LJ, Riggs BL, van Lenthe GH, et al. Contribution of in vivo structural measurements and load/strength ratios to the determination of forearm fracture risk in postmenopausal women. J Bone Miner Res. 2007;22:1442–8.
3. Vico L, Zouch M, Amirouche A, et al. High-resolution pQCT analysis at the distal radius and tibia discriminates patients with recent wrist and femoral neck fractures. J Bone Miner Res. 2008;23:1741–50.
4. Sornay-Rendu E. Severity of vertebral fractures is associated with alterations of cortical architecture in postmenopausal women. J Bone Miner Res. 2009;24:737–43.
5. Wang J, Stein EM, Zhou B, et al. Deterioration of trabecular plate-rod and cortical microarchitecture and reduced bone stiffness at distal radius and tibia in postmenopausal women with vertebral fractures. Bone. 2016;88:39–46.
6. Sornay-Rendu E, Boutroy S, Munoz F, Delmas PD. Alterations of cortical and trabecular architecture are associated with fractures in postmenopausal women, partially independent of decreased BMD measured by DXA: the OFELY study. J Bone Miner Res. 2007;22:425–33.
7. Stein EM, Liu XS, Nickolas TL, et al. Abnormal microarchitecture and reduced stiffness at the radius and tibia in postmenopausal women with fractures. J Bone Miner Res. 2010;25:2296–305.
8. Boutroy S, Khosla S, Sornay-Rendu E, et al. Microarchitecture and peripheral BMD are impaired in postmenopausal Caucasian women with fracture independently of total hip T-score—an International Multicenter Study. J Bone Miner Res. 2016;31:1158–66.
9. MacNeil JA, Boyd SK. Bone strength at the distal radius can be estimated from high-resolution peripheral quantitative computed tomography and the finite element method. Bone. 2008;42:1203–13.
10. Stein EM, Kepley A, Walker M, et al. Skeletal structure in postmenopausal women with osteopenia and fractures is characterized by abnormal trabecular plates and cortical thinning. J Bone Miner Res. 2014;29:1101–9.
11. Vilayphiou N, Boutroy S, Sornay-Rendu E, et al. Finite element analysis performed on radius and tibia HR-pQCT images and fragility fractures at all sites in postmenopausal women. Bone. 2010;46:1030–7.
12. Nishiyama KK, Macdonald HM, Hanley DA, Boyd SK. Women with previous fragility fractures can be classified based on bone microarchitecture and finite element analysis measured with HR-pQCT. Osteoporos Int. 2013;24:1733–40.
13. McCalden R, McGeough J, Barker M, Court-Brown CM. Age-related changes in the tensile properties of cortical bone. The relative importance of changes in porosity, mineralization, and microstructure. J Bone Jt Surg Am. 1993;75:1193–205.
14. Yeni YN, Brown CU, Wang Z, Norman TL. The influence of bone morphology on fracture toughness of the human femur and tibia. Bone. 1997;21:453–9.
15. Burghardt AJ, Buie HR, Laib A, Majumdar S, Boyd SK. Reproducibility of direct quantitative measures of cortical bone microarchitecture of the distal radius and tibia by HR-pQCT. Bone. 2010;47:519–28.
16. Nishiyama KK, Macdonald HM, Buie HR, Hanley DA, Boyd SK. Postmenopausal women with osteopenia have higher cortical porosity and thinner cortices at the distal radius and tibia than women with normal aBMD: an in vivo HR-pQCT study. J Bone Miner Res. 2010;25:882–9.
17. Buie HR, Campbell GM, Klinck RJ, MacNeil JA, Boyd SK. Automatic segmentation of cortical and trabecular compartments based on a dual threshold technique for in vivo micro-CT bone analysis. Bone. 2007;41:505–15.
18. MacDonald HM, Nishiyama KK, Kang J, Hanley DA, Boyd SK. Age-related patterns of trabecular and cortical bone loss differ between sexes and skeletal sites: a population-based HR-pQCT study. J Bone Miner Res. 2011;26:50–62.
19. Vilayphiou N, Boutroy S, Sornay-Rendu E, Van Rietbergen B, Chapurlat R. Age-related changes in bone strength from HR-pQCT derived microarchitectural parameters with an emphasis on the role of cortical porosity. Bone. 2016;83:233–40.
20. Nicks K, Amin S, Atkinson EJ, Riggs BL, Melton LJ III, Khosla S. Relationship of age to bone microstructure independent of areal bone mineral density. J Bone Miner Res. 2012;27:637–44.
21. Garnero P, Sornay-Rendu E, Chapuy M-C., Delmas PD. Increased bone turnover in late postmenopausal women is a major determinant of osteoporosis. J Bone Miner Res. 1996;11:337–49.
22. Arlot ME, Sornay-Rendu E, Garnero P, Vey-Marty B, Delmas PD. Apparent pre- and postmenopausal bone loss evaluated by DXA at different skeletal sites in women: the OFELY cohort. J Bone Miner Res. 1997;12:683–90.
23. Kanis JA, Johnell O, Oden A, Johansson H, McCloskey E. FRAX and the assessment of fracture probability in men and women from the UK. Osteoporos Int. 2008;19:385–97.
24. Genant HK, Wu CY, van Kuijk C, Nevitt MC. Vertebral fracture assessment using a semiquantitative technique. J Bone Miner Res. 1993;8:1137–48.
25. Boutroy S, Bouxsein ML, Munoz F, Delmas PD. In vivo assessment of trabecular bone microarchitecture by high-resolution peripheral quantitative computed tomography. J Clin Endocrinol Metab. 2005;90:6508–15.
26. Laib A, Häuselmann H, Rüegsegger P. In vivo high resolution 3D-QCT of the human forearm. Technol Health Care. 1998;6:329–37.
27. Sode M, Burghardt AJ, Pialat JB, Link TM, Majumdar S. Quantitative characterization of subject motion in HR-pQCT images of the distal radius and tibia. Bone. 2011;48:1291–7.

28. van Rietbergen B, Weinans H, Huiskes R, Odgaard A. A new method to determine trabecular bone elastic properties and loading using micromechanical finite-element models. J Biomech. 1995;28:69–81.
29. Turner CH, Rho J, Takano Y, Tsui TY, Pharr GM. The elastic properties of trabecular and cortical bone tissues are similar: results from two microscopic measurement techniques. J Biomech. 1999;32:437–41.
30. Chiu J, Robinovitch SN. Prediction of upper extremity impact forces during falls on the outstretched hand. J Biomech. 1998;31:1169–76.
31. Stein EM, Liu XS, Nickolas TL, et al. Microarchitectural abnormalities are more severe in postmenopausal women with vertebral compared to nonvertebral fractures. J Clin Endocrinol Metab. 2012;97:1918–26.
32. Bala Y, Zebaze R, Ghasem-Zadeh A, et al. Cortical porosity identifies women with osteopenia at increased risk for forearm fractures. J Bone Miner Res. 2014;29:1356–62.
33. Zebaze R, Ghasem-Zadeh A, Mbala A, Seeman E. A new method of segmentation of compact-appearing, transitional and trabecular compartments and quantification of cortical porosity from high resolution peripheral quantitative computed tomographic images. Bone. 2013;54:8–20.
34. Bjørnerem Å, Bui QM, Ghasem-Zadeh A, Hopper JL, Zebaze R, Seeman E. Fracture risk and height: an association partly accounted for by cortical porosity of relatively thinner cortices. J Bone Miner Res. 2013;28:2017–26.
35. Zebaze RMD, Ghasem-Zadeh A, Bohte A, et al. Intracortical remodelling and porosity in the distal radius and post-mortem femurs of women: a cross-sectional study. Lancet. 2010;375:1729–36.
36. Perilli E, Bala Y, Zebaze R, Reynolds KJ, Seeman E. Regional heterogeneity in the configuration of the intracortical canals of the femoral shaft. Calcif Tissue Int. 2015;97:327–35.
37. Bala Y, Lefèvre E, Roux J-P, et al. Pore network microarchitecture influences human cortical bone elasticity during growth and aging. J Mech Behav Biomed Mater. 2016;63:164–73.
38. Pialat JB, Vilayphiou N, Boutroy S, et al. Local topological analysis at the distal radius by HR-pQCT: application to in vivo bone microarchitecture and fracture assessment in the OFELY study. Bone. 2012;51:362–8.